

ON THE GLOBAL STRUCTURE OF PERIOD DOUBLING FLOWS*

John David CRAWFORD† and Stephen OMOHUNDRO

Lawrence Berkeley Laboratory, University of California, Berkeley, CA 94720, USA

Received 1 December 1983

Revised manuscript received 5 March 1984

For a wide class of period doubling flows on \mathbb{R}^3 , we analyze the global structure of the invariant manifolds and the topology of the bifurcating periodic orbits. We emphasize aspects of the dynamics which are not visible in an analysis of the associated Poincaré return map. The global manifold structure implies constraints for the subsequent bifurcational behavior of the flow. The period doubled orbits are classified using the theory of iterated torus knots. This classification reveals an infinite number of topologically distinct period doubling flows and raises the important question as to which sequences of torus knots appear in the asymptotic limit of a period doubling cascade. If the asymptotic sequence of torus knots produced is not unique, then the self-similarity of the Poincaré map does not imply a self-similar structure for the flow. In particular, at the accumulation point for the cascade, one would not expect to observe a universal power spectrum for the flow. This possibility is of some experimental interest.

1. Introduction

Period doubling transitions occur in physical systems ranging from fluids to electric circuits [1]. They also arise in a host of theoretical models, frequently occurring repeatedly to produce period doubling cascades. These models include maps, such as the logistic map, and differential equations such as the three wave model studied by Wersinger, Finn, and Ott, or the Rössler equations [2].

Most existing theoretical work focuses upon the remarkable universal features of period doubling cascades, and most of this work analyzes maps in one or two dimensions [3]. In contrast to this extensive literature for period doubling in maps, relatively little attention has been devoted explicitly to flows; i.e. solutions of differential equations. In part this is understandable since, by constructing a Poincaré section, a period doubling flow in \mathbb{R}^n defines a period doubling return map in

\mathbb{R}^{n-1} . However, this reduction of a flow to a map eliminates considerable information concerning the global properties of the flow.

In this paper we undertake a study of the global structure of period doubling flows. We are particularly interested in dynamical features, common to any such flow, which persist in the presence of gentle perturbations. Thus our discussion emphasizes topological and geometric properties.

Two issues motivate the analysis. First, for a flow which exhibits period doubling, what is the structure of the invariant manifolds and how does this structure evolve as successive bifurcations occur? Second, how are period doubled orbits embedded in the phase space, and what physically interesting consequences arise from the possibility of different embeddings? Neither of these issues can be satisfactorily addressed using only the Poincaré return maps for the periodic orbits of the flow. For the first question, a detailed knowledge of the flow near fixed points and periodic orbits, and the invariance of stable and unstable manifolds are the essential tools [4]. For the embedding problem we will need simple ideas from the theory of knots [5]. We classify the possible embeddings

*This work was supported by the Office of Basic Energy Sciences of the U.S. Department of Energy under Contract No. DE-AC03-76SF00098.

†Present address: Physics Department, UCSD, La Jolla, CA 92093, USA.

of the period doubled orbits by the type of torus knot produced.

Period doubling flows do not exist in fewer than three dimensions; thus to begin with the simplest case, we shall discuss vector fields, $X_\mu(x)$, on \mathbb{R}^3 which define a differential equation in the usual way:

$$\dot{x} = X_\mu(x), \quad x \in \mathbb{R}^3, \quad \mu \in \mathbb{R}. \quad (1a)$$

As indicated, $X_\mu(x)$ depends on a parameter μ ; for convenience we assume a fixed point at $x = x_0$.

$$X_\mu(x_0) = 0 \quad (1b)$$

As μ varies, the flow generated by X_μ varies. We consider the sequence of events shown in fig. 1: a stable node at x_0 becomes a stable spiral node, the spiral node loses stability through a Hopf bifurcation which produces a limit cycle, in a Poincaré section for the limit cycle, the stable node corresponding to the limit cycle becomes a stable spiral node, and finally the Hopf orbit loses stability through a period doubling bifurcation. This sequence is observed in both the Rössler equations and the three wave equations mentioned above. In sections 2 and 3, we analyze these transitions by explicitly constructing a simple one parameter family of vector fields, denoted $V_\mu(x)$, with the desired behavior. This construction is summarized in Table I. The simplicity of $V_\mu(x)$ allows a detailed global analysis; this is the primary motivation for its construction.

The qualitative features of $V_\mu(x)$ are shared by all nearby period doubling flows because it is a structurally stable family [4]. This is a significant point which we briefly and heuristically elaborate. Imagine the space composed of all smooth vector fields on \mathbb{R}^3 ; any one parameter family of vector fields determines a curve through this space. We construct a particular path, $V_\mu(x)$, which connects three different subsets of vector fields, see fig. 2. Our path begins in the subset of vector fields with a stable fixed point x_0 , then crosses into the subset of vector fields with an unstable fixed point x_0

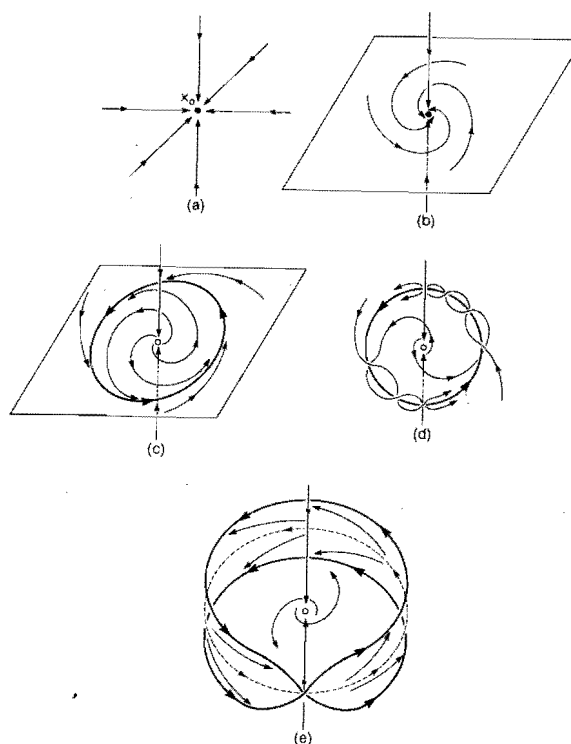


Fig. 1. The qualitative features of Hopf bifurcation and period doubling. a) a single attracting fixed point; b) invariant plane with spiral flow; c) recently born Hopf limit cycle; d) flow spirals around limit cycle; e) recently born period doubled orbit lies on the edge of a Möbius strip and original Hopf orbit (dashed) is unstable.

and a stable periodic orbit, and finally crosses into the set of vector fields with an unstable fixed point x_0 , an unstable periodic orbit, and a stable orbit (with approximately twice the period of the unstable orbit). The boundaries of these sets are bifurcation surfaces corresponding to Hopf bifurcation, Σ_1 , and period doubling, Σ_2 . Our path crosses these surfaces transversally. Off Σ_1 and Σ_2 , each vector field in our constructed family generates a structurally stable flow whose topological features will survive under perturbation. On Σ_1 and Σ_2 , the flows are structurally unstable, but the family containing these flows is stable because the crossings are transverse. Hence a nearby family, $V_\mu + \delta V_\mu$, will also cross Σ_1 and Σ_2 and thus qualitatively resemble $V_\mu(x)$.

Table I

Parameter Range	Form of V_μ	Comments
$\mu \leq \mu_1$	$\dot{x} = \lambda_1(\mu)x$ $\dot{y} = \lambda_2(\mu)y$ $\dot{z} = \lambda(\mu)z$	$\lambda, \lambda_1, \lambda_2 < 0$ $\lambda_1(\mu_1) = \lambda_2(\mu_1)$
$\mu_1 \leq \mu \leq \mu_2$	$\dot{r} = v(\mu)r$ $\dot{\theta} = \omega(\mu)$ $\dot{z} = \lambda(\mu)z$	$v = \text{Re } \lambda_1 < 0$ $\omega = \text{Im } \lambda_1; \omega(\mu_1) = 0; \omega(\mu_2) = 1$ $\lambda < 0$
$\mu_2 \leq \mu \leq \mu_3$	$\dot{r} = vr - S(\mu)r^3$ $\dot{z} = \lambda(\mu)z$ $\dot{\theta} = 1$	$\lambda, v < 0$ $S(\mu) = \begin{cases} 0, & \mu \leq \mu_2 \\ 1, & \mu \geq \mu_3 \end{cases}$
$\mu_3 \leq \mu \leq \mu_4$	$\dot{r} = v(\mu)r - r^3$ $\dot{z} = \lambda z$ $\dot{\theta} = 1$	$\lambda < 0, v' > 0$ $v < 0$ for $\mu \leq \mu_3$ $v > 0$ for $\mu \geq \mu_4$
For $\mu \geq \mu_4$	$V_\mu = (1 - S(\sigma))V_{\mu_4} + S(\sigma)V_\mu^T$ Form of V_μ^T	
$\mu = \mu_4$	$\dot{\rho} = -2v(\mu)\rho - \rho^2(3\sqrt{v} + \rho)$ $\dot{z} = \lambda(\mu)z$ $\dot{\theta} = 1$	
$\mu_4 \leq \mu \leq \mu_5$	$\dot{\rho} = -2v\rho - S(\mu)\rho^2(3\sqrt{v} + \rho)$ $\dot{z} = \lambda z$ $\dot{\theta} = 1$	$v > 0, \lambda < 0$ $S(\mu) = \begin{cases} 1, & \mu \leq \mu_4 \\ 0, & \mu > \mu_5 \end{cases}$
$\mu_5 \leq \mu \leq \mu_6$	$\dot{\rho} = -2v\rho$ $\dot{z} = \lambda z$ $\dot{\theta} = 1$	$\lambda, -2v < 0$ $\lambda(\mu_6) = -2v(\mu_6)$
$\mu_6 \leq \mu \leq \mu_7$	$\dot{\sigma} = \eta(\mu)\sigma$ $\dot{\phi} = \Delta(\mu)$ $\dot{\theta} = 1$	$\eta < 0, \eta(\mu_6) = \lambda(\mu_6)$ $\Delta(\mu_6) = 0, \Delta(\mu_7) = \frac{1}{2}$ $\Delta' > 0$
$\mu_7 \leq \mu \leq \mu_8$	$\dot{\sigma} = \eta\sigma + S(\mu)\sigma \left[(\alpha - \eta) \sin^2 \left(\phi - \frac{\theta}{2} \right) - \sigma^2 \cos^4 \left(\phi - \frac{\theta}{2} \right) \right]$ $\dot{\phi} = \frac{1}{2} + \frac{S(\mu) \sin 2(\phi - \theta/2)}{2} \left[\alpha - \eta + \sigma^2 \cos^2 \left(\phi - \frac{\theta}{2} \right) \right]$ $\dot{\theta} = 1$	$\eta, \alpha < 0$ $\eta(\mu_7) = \alpha(\mu_7)$ $S(\mu) = \begin{cases} 0, & \mu \leq \mu_7 \\ 1, & \mu > \mu_8 \end{cases}$
$\mu_8 \leq \mu \leq \mu_9$	$\dot{\sigma} = \eta\sigma + \sigma \left[(\alpha - \eta) \sin^2 \left(\phi - \frac{\theta}{2} \right) - \sigma^2 \cos^4 \left(\phi - \frac{\theta}{2} \right) \right]$ $\dot{\phi} = \frac{1}{2} + \frac{\sin 2(\phi - \theta/2)}{2} \left[(\alpha - \eta) + \sigma^2 \cos^2 \left(\phi - \frac{\theta}{2} \right) \right]$ $\dot{\theta} = 1$	$\eta(\mu_8) < 0$ $\eta(\mu_9) > 0$ $\eta'(\mu) > 0$ $\alpha < 0$

After the construction of $V_\mu(x)$ we draw the invariant manifolds in section 4. These manifolds, by virtue of their invariance, organize the global flow; they can also constrain the subsequent bifurcational behavior of the family. An example of such global constraints is described in section 5. In section 6, the topology of the period doubled orbits is analyzed. In \mathbb{R}^3 , period doubling produces orbits which are torus knots. In sections 7 and 8, we discuss the physical consequences of different orbit topologies. If the sequence of torus knots which appears in the asymptotic regime of a period doubling cascade is not unique, then not all of the universal features of period doubling Poincaré maps [3] will be inherited by the flow. Specifically, the asymptotic flow could fail to be self similar, and the power spectrum of the flow need not satisfy universal scaling laws [12].

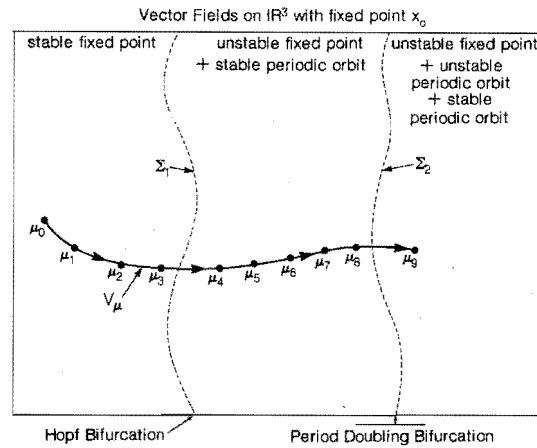


Fig. 2. Schematic representation of the infinite dimensional space of vector fields with one-parameter family shown puncturing the Hopf and period doubling bifurcation surfaces Σ_1 and Σ_2 .

2. Hopf bifurcation

Our prototypical family of vector fields will be defined by giving a coordinate representation of $V_\mu(x)$ for each interval in μ shown in fig. 3. The coordinate systems we require appear in fig. 4.

To begin let $V_{\mu_0}(x)$ be a vector field on \mathbb{R}^3 with a stable node at $x = 0$. This means the eigenvalues of the matrix

$$(DV_{\mu_0}(0))_{ij} = \frac{\partial V_{\mu_0}^i}{\partial x^j}(0), \quad i, j = 1, 2, 3,$$

are real-valued and negative. For $x = 0$ to lose stability in a Hopf bifurcation, $DV_\mu(0)$ must have a complex conjugate pair of eigenvalues which cross the imaginary axis into the right half of the complex plane [4, 6]. To produce such a pair, two of the initially real eigenvalues must collide and leave the real axis; let $\mu = \mu_1$ be the parameter value for this collision. In coordinates, for $\mu \leq \mu_1$, $V_\mu(x)$ can be simply taken to be linear,

$$\begin{aligned} \mu \leq \mu_1 \quad \dot{x} &= \lambda_1(\mu)x, \quad \lambda, \lambda_1, \lambda_2 < 0, \\ \dot{y} &= \lambda_2(\mu)y, \quad \lambda_1 = \lambda_2 \quad \text{at } \mu = \mu_1, \\ \dot{z} &= \lambda(\mu)z. \end{aligned}$$

After the collision λ_1 and λ_2 form a conjugate pair of eigenvalues, $\nu(\mu) \pm i\omega(\mu)$, and the node becomes a spiral node; polar coordinates are now convenient. We normalize time so that for $\mu \geq \mu_2$ the angular velocity $\omega(\mu)$ is unity. Thus on $\mu_1 \leq \mu \leq \mu_2$, V_μ is

$$\begin{aligned} \mu_1 \leq \mu \leq \mu_2 \quad r &= \nu(\mu)r, \quad \nu = \operatorname{Re} \lambda_1 < 0, \\ \dot{\theta} &= \omega(\mu), \quad \omega = \operatorname{Im} \lambda_1; \omega(\mu_1) = 0, \quad \omega(\mu_2) = 1, \\ \dot{z} &= \lambda(\mu)z, \quad \lambda < 0. \end{aligned}$$

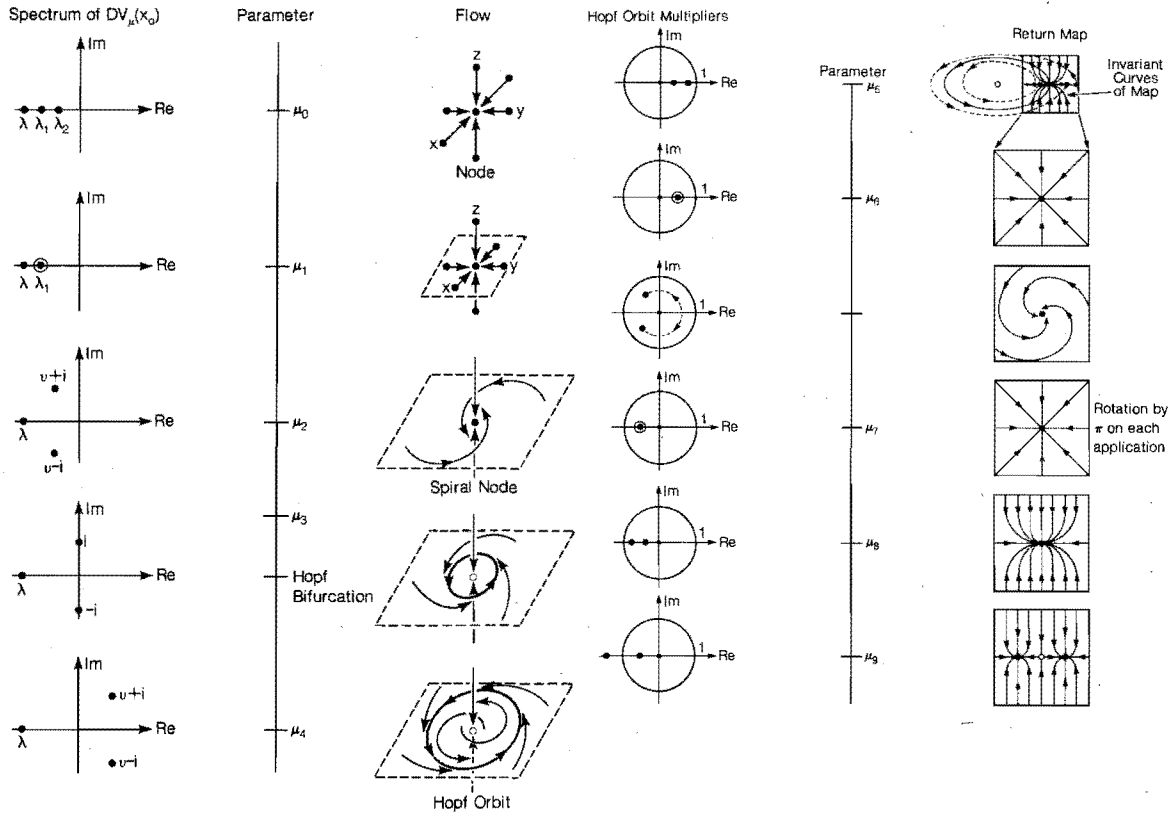


Fig. 3a. At left, the eigenvalue spectrum of the linearized vector field at the fixed point and key features of the flow for parameter values μ_0 to μ_4 .

Fig. 3b. At right, the eigenvalue spectrum of the linearized Poincaré return map and invariant curves in the surface of section for parameter values μ_5 to μ_9 .

When $v(\mu)$ changes sign, if the Hopf bifurcation is to produce a stable limit cycle, the \dot{r} equation needs an r^3 term to balance the repulsion at $r = 0$. Such a term can be “spliced” into $V_\mu(x)$ using the simple device of turning on r^3 with a smooth step function, $S(\mu)$, see fig. 5. Once the r^3 term is in place, allowing $v(\mu)$ to increase through zero yields the desired Hopf bifurcation. These extensions of $V_\mu(x)$ are explicitly made as follows:

$$\begin{aligned}
 \mu_2 \leq \mu \leq \mu_3 \quad & \dot{r} = v(\mu)r - S(\mu)r^3, \quad \lambda, v < 0, \\
 \dot{z} &= \lambda(\mu)z, \quad S(\mu) = \begin{cases} 0, & \mu \leq \mu_2, \\ 1, & \mu \geq \mu_3; \end{cases} \\
 \dot{\theta} &= 1, \\
 \mu_3 \leq \mu \leq \mu_4 \quad & \dot{r} = v(\mu)r - r^3, \quad v(\mu) < 0 \text{ for } \mu \leq \mu_3, \\
 \dot{z} &= \lambda(\mu)z, \quad v(\mu) > 0 \text{ for } \mu \geq \mu_4, \\
 \dot{\theta} &= 1, \quad v'(\mu) > 0 \text{ for } \mu_3 < \mu < \mu_4.
 \end{aligned}$$

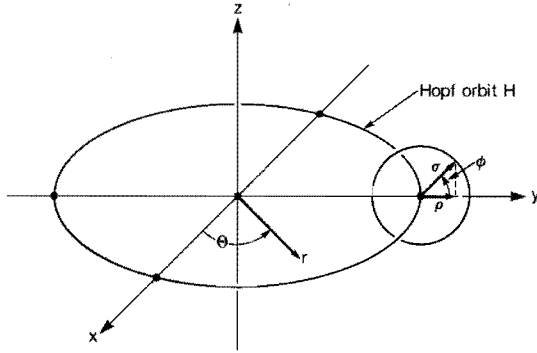


Fig. 4. The four coordinate systems used: (x, y, z) , (r, θ, z) , (ρ, θ, z) , (σ, ϕ, θ) .

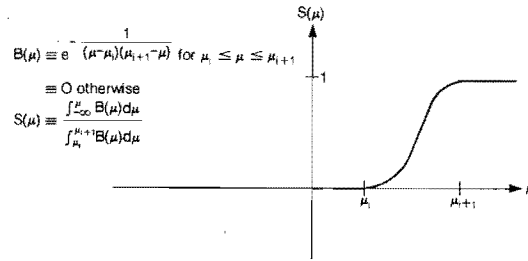


Fig. 5. The smooth step function $S(\mu)$ constructed from the bump $B(\mu)$.

The flow obtained from $V_\mu(x)$ for $\mu \leq \mu_4$ is shown in fig. 3a. The Hopf bifurcation occurs for some value $\mu = \mu_H$ in the interval (μ_3, μ_4) . The above assumptions about $\nu(\mu)$ on this interval assure the curve of vector fields V_μ will cross the surface Σ_1 transversally, see fig. 2.

In the next section, the period doubling of the Hopf orbit will be discussed. To simplify the local analysis of this bifurcation, we introduce new coordinates near the limit cycle and “freeze” the flow away from the limit cycle. For $\nu(\mu) > 0$ the Hopf orbit has radius $r_H = \sqrt{\nu}$, if we shift to coordinates centered on the orbit, $r \rightarrow \rho + r_H$, then $V_{\mu_4}(x)$ can be rewritten,

$$\begin{aligned} \mu &= \mu_4 & \dot{\rho} &= -2\nu\rho - (3\sqrt{\nu} + \rho)\rho^2, \\ & & \dot{z} &= \lambda z, \\ & & \dot{\theta} &= 1. \end{aligned} \quad (2)$$

To clearly single out the flow near $\rho = 0$, choose two concentric tori which enclose the orbit. In terms of the local radial coordinate, $\sigma = \sqrt{\rho^2 + z^2}$, denote the interior radii of these tori by σ_1 and σ_2 with $\sigma_2 > \sigma_1$ as shown in fig. 6. Now use a smooth step function, $S(\sigma)$, to split $V_\mu(x)$ into two pieces for $\mu \geq \mu_4$:

$$V_\mu(x) = (1 - S(\sigma))V_{\mu_4}(x) + S(\sigma)V_\mu^T(x), \quad (3)$$

where

$$S(\sigma) = \begin{cases} 1, & \sigma \leq \sigma_1, \\ 0, & \sigma \geq \sigma_2, \end{cases}$$

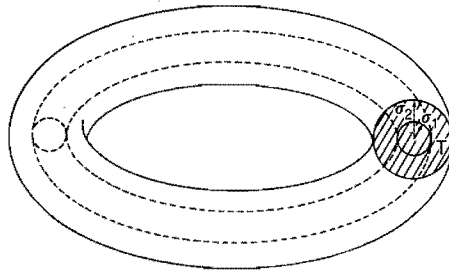


Fig. 6. The toroidal region T.

and $V_{\mu_4}^T$ is given by eq. (2). At $\mu = \mu_4$, eq. (3) obviously reduces to $V_\mu(x)$ as previously defined. As μ increases past μ_4 only $V_\mu^T(x)$, the piece of $V_\mu(x)$ on the interior of the toroidal region T , will be allowed to vary. Thus the period doubling behavior will be contained in V_μ^T , leaving the exterior flow unperturbed. This arrangement facilitates the global analysis of section 4.

3. Period doubling

As a preliminary step, the nonlinearity of $V_\mu^T(x)$ in eq. (3) is removed using the (now familiar) device of a smooth step function $S(\mu)$,

$$\begin{aligned} \mu_4 \leq \mu \leq \mu_5 \quad \dot{\rho} &= -2\nu\rho - S(\mu)(3\sqrt{\nu} + \rho)\rho^2, \quad \nu > 0, \quad \lambda < 0 \\ \dot{z} &= \lambda z, \quad S(\mu) = \begin{cases} 1, & \mu \leq \mu_4, \\ 0, & \mu \geq \mu_5. \end{cases} \\ \dot{\theta} &= 1, \end{aligned}$$

At $\mu = \mu_5$, the Hopf orbit is a global attractor; its linear stability is determined by the Floquet multipliers of the linearization of $V_\mu^T(x)$ at $\rho = 0$, or equivalently by the exponents of the linearized Poincaré return map. The multipliers are $e^{2\pi\lambda}$ and $e^{-4\pi\nu}$; both are real and less than unity. In the associated return map, the orbit appears as a stable node.

A period doubling bifurcation requires a multiplier to leave the unit disk of the complex plane through -1 [4]. Producing a negative multiplier requires that the positive multipliers collide, move into the complex plane as a conjugate pair, circle the origin, and collide again on the negative real axis. Let the first collision occur at $\mu = \mu_6$, i.e. $\lambda(\mu_6) = -2\nu(\mu_6)$; denote by μ_7 the parameter value of the second collision. For $\mu > \mu_6$ the stable node in the return map becomes a stable spiral node, and it is simplest to work in the local polar variables: $\sigma^2 = z^2 + \rho^2$ and $\phi = \tan^{-1}(z/\rho)$. On $\mu_5 \leq \mu \leq \mu_7$, $V_\mu^T(x)$ has the form,

$$\begin{aligned} \mu_5 \leq \mu \leq \mu_6 \quad \dot{\rho} &= -2\nu\rho, \quad \lambda, -2\nu < 0, \\ \dot{z} &= \lambda z, \quad \lambda(\mu_6) = -2\nu(\mu_6); \\ \dot{\theta} &= 1, \\ \mu_6 \leq \mu \leq \mu_7 \quad \dot{\sigma} &= \eta(\mu)\sigma, \quad \eta < 0, \eta(\mu_6) = \lambda(\mu_6), \\ \dot{\phi} &= \Delta(\mu), \quad \Delta(\mu_6) = 0, \Delta(\mu_7) = 1/2, \\ \dot{\theta} &= 1, \quad \Delta'(\mu) \geq 0; \\ \mu = \mu_7 \quad \dot{\sigma} &= \eta(\mu_7)\sigma, \\ \dot{\phi} &= 1/2, \\ \dot{\theta} &= 1. \end{aligned}$$

At $\mu = \mu_7$, the Hopf orbit is still attracting, but now the flow near the orbit executes a half twist in ϕ for every full revolution in θ †. The multipliers are both equal to $-e^{2\pi\eta}$.

As for the Hopf bifurcation, the period doubling bifurcation requires nonlinear terms to balance the repulsion from the Hopf orbit and allow a stable period doubled orbit to appear. An appropriate form for these terms can be derived by considering first a pitchfork bifurcation from a fixed point for a two

†Note that the linearized Poincaré map at μ_6 and μ_7 has the form $\begin{pmatrix} \lambda & 0 \\ 0 & \lambda \end{pmatrix}$. Small perturbations can make this $\begin{pmatrix} \lambda & 0 \\ \epsilon & \lambda \end{pmatrix}$ but this does not qualitatively change the flow.

dimensional flow on the (z, ρ) -plane, at $\theta = 0$. This flow is described by

$$\begin{aligned} \dot{z} &= \alpha z, & \alpha < 0, \\ \dot{\rho} &= \rho(\eta - \rho^2), & \eta < 0, \quad \eta' > 0. \end{aligned}$$

For $\eta < 0$ there is one (stable) fixed point at $(z, \rho) = (0, 0)$ which will correspond to the Hopf orbit. For $\eta > 0$, $(0, 0)$ is unstable and new stable fixed points appear at $(0, \pm \sqrt{\eta})$. These will correspond to the period doubled orbit. In terms of σ and ϕ , this two dimensional flow is

$$\begin{aligned} \dot{\sigma} &= \eta\sigma + \sigma[(\alpha - \eta)\sin^2\phi - \sigma^2\cos^4\phi], \\ \dot{\phi} &= \frac{1}{2}(\alpha - \eta + \sigma^2\cos^2\phi)\sin 2\phi. \end{aligned}$$

Now to return to three dimensions and realize a period doubling bifurcation, this two dimensional flow must be swept around the Hopf orbit in the coordinate θ with a simultaneous rotation in the angle ϕ given by $\theta/2$: $\phi \rightarrow \phi - \theta/2$. Thus putting $\dot{\theta} = 1$ back in yields,

$$\begin{aligned} \dot{\sigma} &= \eta\sigma + \sigma[(\alpha - \eta)\sin^2(\phi - \theta/2) - \sigma^2\cos^4(\phi - \theta/2)], \\ \dot{\phi} &= \frac{1}{2} + \frac{1}{2}[\alpha - \eta + \sigma^2\cos^2(\phi - \theta/2)]\sin 2(\phi - \theta/2), \\ \dot{\theta} &= 1, \end{aligned}$$

which gives the form of the desired nonlinear terms for period doubling. Again these nonlinear terms are added using a step function, so we extend $V_\mu^T(x)$ by

$$\begin{aligned} \mu_7 \leq \mu \leq \mu_8 \quad \dot{\sigma} &= \eta(\mu)\sigma + S(\mu)\sigma[(\alpha - \eta)\sin^2(\phi - \theta/2) - \sigma^2\cos^4(\phi - \theta/2)], \\ \dot{\phi} &= \frac{1}{2} + \frac{S(\mu)}{2}[\alpha - \eta + \sigma^2\cos^2(\phi - \theta/2)]\sin 2(\phi - \theta/2), \\ \dot{\theta} &= 1, \end{aligned}$$

with

$$S(\mu) = \begin{cases} 0, & \mu \leq \mu_7, \\ 1, & \mu \geq \mu_8, \end{cases}$$

and

$$\eta, \alpha < 0 \quad \eta(\mu_7) = \alpha(\mu_7).$$

Note that the multipliers are $-e^{2\pi\eta}$ and $-e^{2\pi\alpha}$.

Period doubling occurs when η increases through zero. For $\mu \geq \mu_8$ define $V_\mu^T(x)$ by

$$\begin{aligned} \mu_8 \leq \mu \leq \mu_9 \quad \dot{\sigma} &= \eta\sigma + \sigma \left[(\alpha - \eta) \sin^2 \left(\phi - \frac{\theta}{2} \right) - \sigma^2 \cos^4 \left(\phi - \frac{\theta}{2} \right) \right], \\ \dot{\phi} &= \frac{1}{2} + \frac{1}{2} \left[\alpha - \eta + \sigma^2 \cos^2 \left(\phi - \frac{\theta}{2} \right) \right] \sin 2 \left(\phi - \frac{\theta}{2} \right), \\ \dot{\theta} &= 1, \end{aligned} \quad (4)$$

where $\eta(\mu_8) < 0$, $\eta(\mu_9) > 0$, $\eta'(\mu) > 0$. These conditions on η ensure that the bifurcation surface Σ_2 is crossed transversally.

4. Local to global

In the previous two sections a strictly local analysis guided us in the construction of $V_\mu(x)$. By virtue of this construction the flow is well understood in the neighborhood of each fixed point or periodic orbit. Because $V_\mu(x)$ is defined on all of \mathbb{R}^3 , we can now patch together these local pictures and obtain a global description [14]. One of the most important global aspects of a dynamical system is the structure of the stable and unstable manifolds of the hyperbolic fixed points and closed orbits. Recall that a fixed point is hyperbolic if the matrix of the linearized vector field has no eigenvalues on the imaginary axis and a closed orbit is hyperbolic if the matrix representing the linearized Poincaré map has no eigenvalues on the unit circle in the complex plane. For hyperbolic fixed points (or closed orbits) the stable manifold is the set of points which asymptotically approach the point (or orbit) as time goes to positive infinity. The unstable manifold is the set of points which have this asymptotic approach as time goes to negative infinity. One of the key mathematical results of dynamical systems theory is that these sets are in fact smoothly immersed submanifolds [7]. For the case of fixed points they are tangent to the corresponding stable or unstable linear eigenspace and have dimension equal to that of the eigenspace. For periodic orbits the relevant linear eigenspaces are those associated with the linearized Poincaré map. The intersection of the invariant manifolds

with the Poincaré section defines surfaces which are tangent to and of the same dimension as the appropriate eigenspace. The invariant manifolds themselves are one dimension larger than this intersection.

In the case at hand, $V_{\mu_9}(x)$, we have one unstable fixed point P and two periodic orbits: the unstable Hopf orbit H and the stable period doubled orbit L (see fig. 7). Since L is stable, its stable manifold is all of \mathbb{R}^3 except for the stable manifolds of H and P . L 's unstable manifold is just L itself. It is easy to determine P 's manifolds outside the region T because the flow there has not changed since the Hopf bifurcation at $\mu \approx \mu_4$. As in fig. 8, P 's stable manifold is just the z -axis. Outside of T its unstable manifold is a 2-dimensional disc in the x - y plane which intersects the boundary of the toroidal region T in a circle C_1 .

Before considering P 's unstable manifold inside the region T we will describe the manifolds for the unstable orbit H inside T . The Poincaré section of

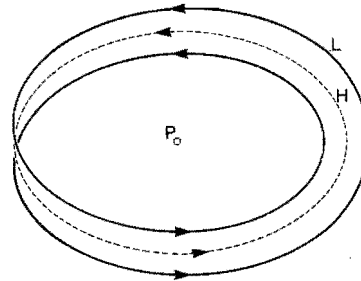


Fig. 7. The fixed point P , the Hopf orbit H and the period doubled orbit L .

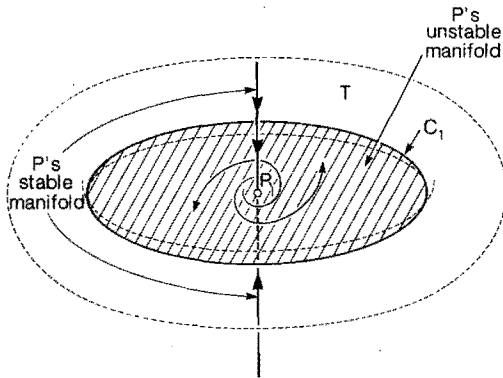


Fig. 8. P's stable manifold, its unstable manifold outside T, and its intersection C_1 with T's boundary.

the flow inside T was determined earlier for the single slice $\theta = 0$ (fig. 3b). At any other value of θ we get the same picture rotated in ϕ by an angle $\theta/2$ (fig. 9). Thus a full rotation in θ produces a half twist in ϕ . Within each Poincaré section defined by a given θ , the fixed point of the Poincaré

map corresponding to H has stable and unstable manifolds. The unions over θ of these manifolds yield the corresponding stable and unstable manifolds for the entire orbit H. Thus in fig. 10 we see that the unstable manifold of H is a Möbius strip, contained in T, whose boundary is the stable orbit L [8]. The portion of H's stable manifold contained in T is also a Möbius strip, perpendicular to the unstable manifold (fig. 11). We would like to know what happens to it as it protrudes out of T. Note that it intersects the boundary of T in a circle C_2 that winds around T twice in the θ direction.

The key notion which allows us to complete these descriptions is that the stable and unstable manifolds are invariant under the flow. This invariance is clear from their definition. Invariance implies that the portion of P's unstable manifold that lies inside T is exactly the surface swept out by the circle C_1 under the flow. In fig. 12 we see how C_1 intersects the plane defined by $\theta = 0$ as it

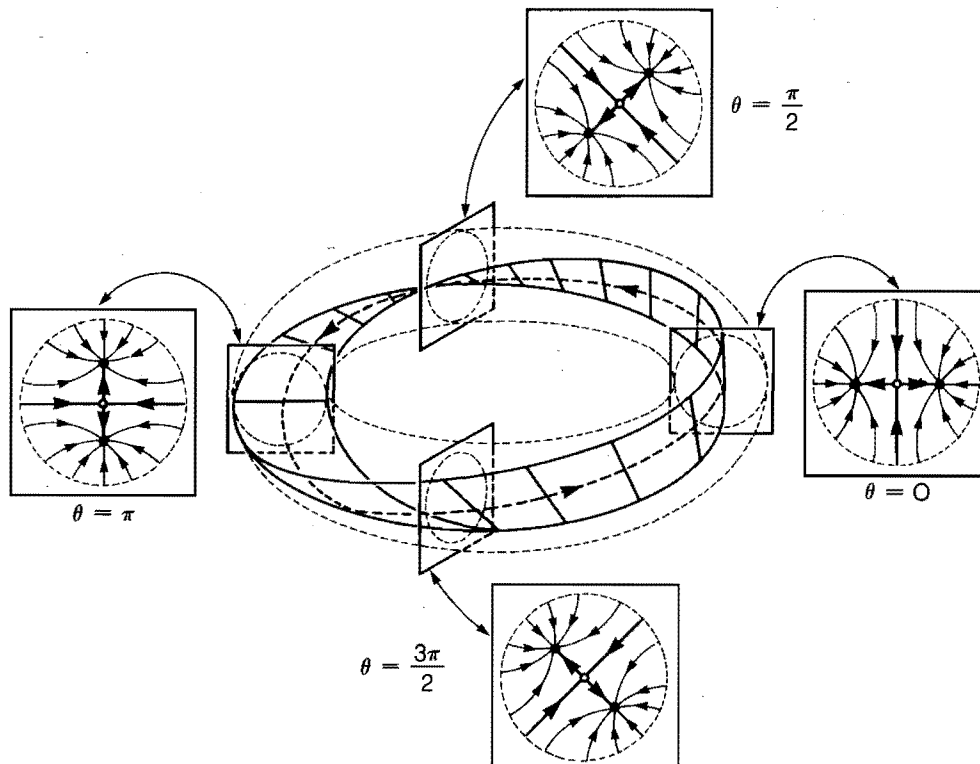


Fig. 9. Poincaré sections at $\theta = 0, \pi/2, \pi, 3\pi/2$ inside T. For the flow, the Hopf orbit and its local stable manifold are shown. The period doubled orbit is not explicitly drawn.

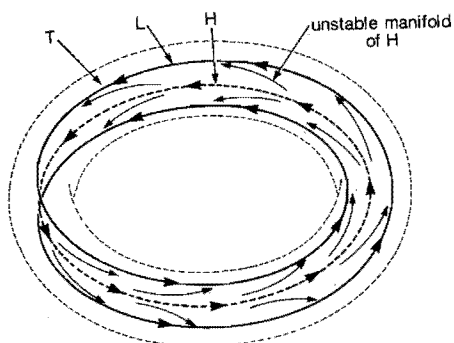
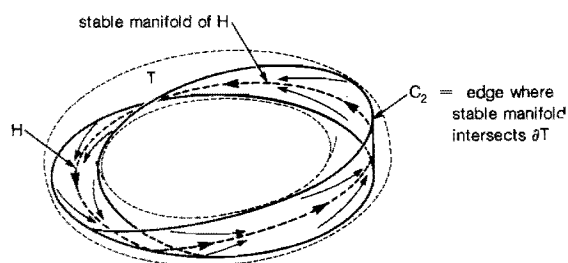
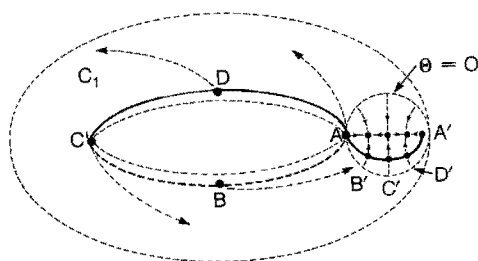


Fig. 10. H's unstable manifold.

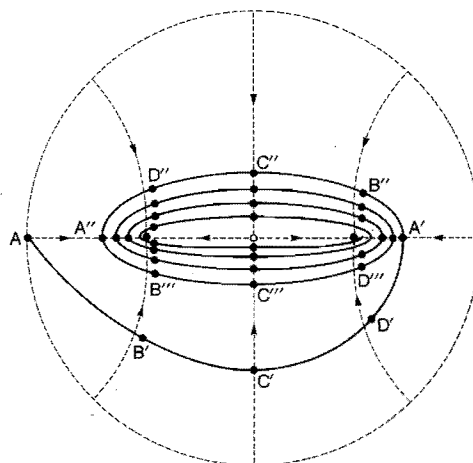
Fig. 11. H's stable manifold inside T and its intersection C_2 with T's boundary.Fig. 12. The circle C_1 evolves under the flow and the first points of intersection with $\theta = 0$ are indicated.

evolves under the flow. Point A is already in this plane. The orbit through B hits the plane at a point B' which is displaced radially inward and rotated in ϕ . Similarly, orbits through C and D hit the plane at C' and D' . Finally, the orbit through A returns to the plane at A' ; this is of course the image of A under the Poincaré map.

In fig. 13 we continue to follow the image of C_1 under the flow and show the intersection of P's unstable manifold inside T with the plane $\theta = 0$. At any other θ we get the same picture rotated by $\theta/2$. As before the entire unstable manifold in T is the union of these fixed θ slices. Half of the resulting "pie-crust" structure is shown in fig. 14. Notice that P's unstable manifold wraps around and limits on the whole Möbius strip (H's unstable manifold).

A similar construction for the exterior of T gives the stable manifold of the unstable orbit H. Here though we take the curve C_2 and let it evolve backward in time. The resulting stable manifold is

shown in fig. 15. At first, it may be surprising that the stable manifold has a spiral structure in ϕ , while the flow outside T spirals only in the θ direction. This is however a simple consequence of

Fig. 13. The intersection of $\theta = 0$ with the surface swept out by C_1 's evolution.

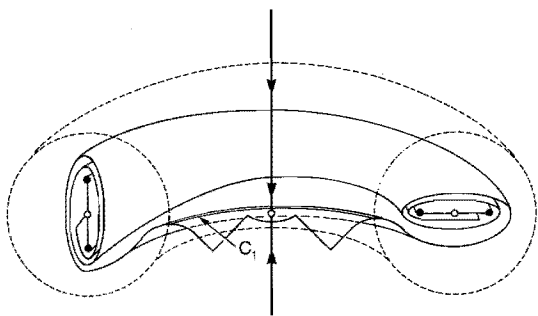


Fig. 14. P's unstable manifold.

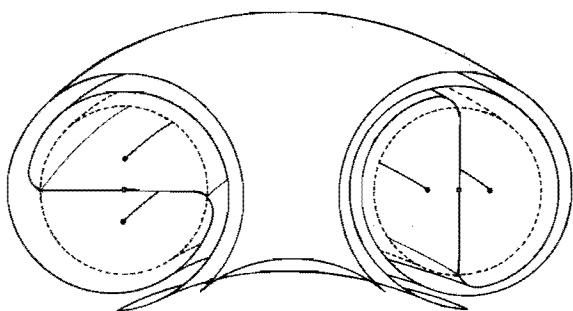


Fig. 15. H's stable manifold.

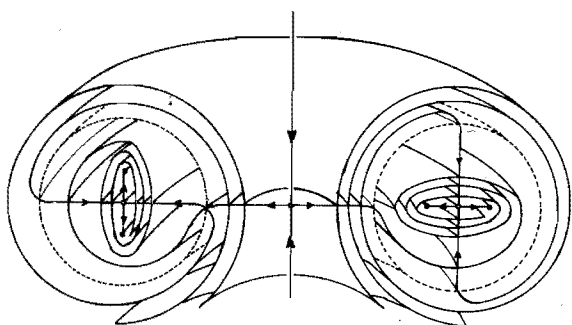


Fig. 16. P's and H's stable and unstable manifolds showing transversal intersection.

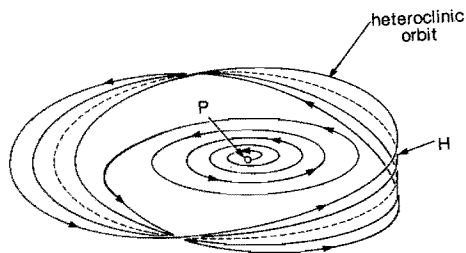


Fig. 17. The heteroclinic orbit from P to H.

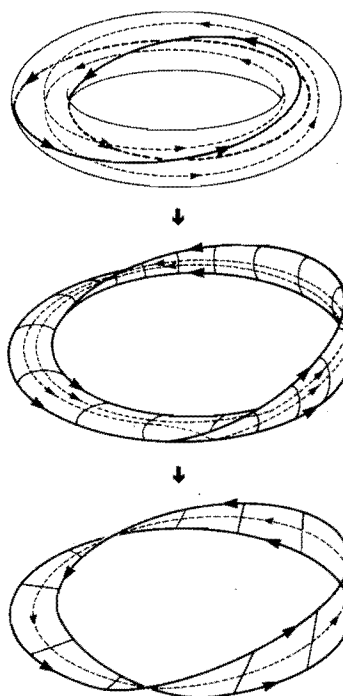


Fig. 18. 2:1 phase-locked flow on a torus being compressed to the Möbius strip unstable manifold of an unstable periodic orbit with stable period doubled orbit. The light dotted orbit is unstable, and the dark solid orbit is stable. At top, both have the same period; on the Möbius band below, the dotted orbit has become the Hopf orbit with half the period of the solid orbit.

the fact that the Möbius structure inside T spirals in ϕ as you rotate it in θ . Note that this manifold limits on the whole line of P's stable manifold. The tightly bunched structure of H's stable manifold near P means that small changes in the initial conditions of orbits passing near P lead to large differences in the "phase" with which these orbits approach L. To see this consider the square of the Poincaré map for the section $\theta = 0$, the two points where L intersects this plane are attracting fixed points for this map. The basins of attraction for these fixed points are separated by the intersection of H's stable manifold with this plane.

In fig. 16 we draw the two manifolds simultaneously and see that they do indeed intersect transversally. Their intersection is a heteroclinic orbit (fig. 17) spiralling out from P and limiting on H from two sides.

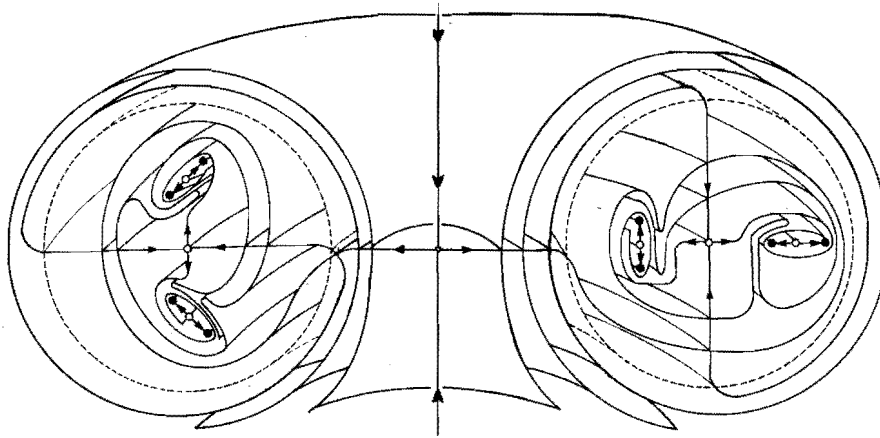


Fig. 19. The invariant manifolds at the second stage of period doubling.

It may be helpful to the reader to think of the Möbius strip formed by L and H's unstable manifold as a squashed version of a torus (fig. 18) with the toral flow in 2:1 phase locking. This shows geometrically how period doubling resembles a secondary Hopf bifurcation resonant with the primary Hopf bifurcation.

Similar arguments to the above apply to subsequent period doubling bifurcations of L. To construct the k th period doubling surround the limit cycle produced by the $k-1$ st period doubling bifurcation by a toroidal region. The Grobman-Hartman theorem lets us choose this region small enough that the interior flow is topologically the same as that of eq. (4). Now, as described in section 3 change the flow only in this toroidal neighborhood. For example, after two period doublings we get fig. 19. This process may be iterated a finite number of times, but whether an entire period doubling cascade can occur in such a simple fashion is unclear [14].

5. Implications for subsequent bifurcations

In this section we briefly indicate how the global structure just discussed can influence the subsequent bifurcational behavior of the period doubled orbit. The general problem of tracing families of periodic orbits in \mathbb{R}^3 has also been discussed re-

cently by Alexander and Yorke [15]. We have a particular class of systems in mind: flows in \mathbb{R}^3 with strong dissipation, i.e.

$$\operatorname{div} V_\mu(x) < 0, \quad x \in \mathbb{R}^3, \quad (5)$$

which have undergone a period doubling bifurcation, and therefore possess the Möbius strip invariant manifold structure described above. We also assume, for simplicity, that in the period doubling parameter regime the number of fixed points remains constant.† Examples of models in this class are damped, driven oscillators and the three wave system [2, 9].

As the parameter μ is varied, in the absence of special symmetries or other “non-generic” properties of $V_\mu(x)$, what subsequent bifurcations are expected from the period doubled orbit? (One uninteresting possibility is that the orbit could “back up”, and collapse onto the Hopf orbit in an inverse period doubling bifurcation. We assume this does not happen.) The possible bifurcations may be enumerated by the behavior of the Floquet multipliers of the period doubled orbit. These pos-

†By allowing the creation and destruction of fixed points (in saddle-node bifurcations) to occur along the unstable center orbit of the Möbius band, Alexander and Yorke (ref. 15) devised a global bifurcation which unlinks the Hopf orbit and the period doubled orbit.

sibilities are threefold:

- 1) a complex conjugate pair of multipliers, $\rho_1 = \bar{\rho}_2$, crosses the unit circle;
- 2) a real multiplier crosses the unit circle at $+1$;
- 3) a real multiplier crosses the unit circle at -1 .

The first possibility is ruled out by the strong dissipation assumption. This follows from the relationship between the two nontrivial Floquet multipliers, ρ_1 and ρ_2 , and the trace of $DV_\mu(x)$ averaged over the orbit;

$$\rho_1 \rho_2 = \exp \left[\int_0^T \text{Tr} DV_\mu(x(t)) dt \right].$$

Here $x(t)$ represents the period doubled orbit with period T [10]. Since

$$\text{Tr} DV_\mu(x(t)) = \text{div} V_\mu(x(t)) < 0,$$

we have

$$\rho_1 \rho_2 = \exp \left[\int_0^T \text{div} V_\mu(x(t)) dt \right] < 1,$$

which precludes a conjugate pair of multipliers from reaching the unit circle. It is clear at this point that the assumption in eq. (5) could be weakened to

$$\int_0^T \text{div} V_\mu(x(t)) dt < 0. \quad (6)$$

In this form our discussion also applies to the Rössler system [2].

The second possibility generically yields a saddle-node bifurcation in which the stable orbit (the node) collides with an unstable orbit (the saddle) and both disappear [4]. For this bifurcation the twisted invariant manifolds, associated with the stable period doubled orbit, play an important role. The twisted structure of the Möbius band forces the stable period doubled orbit to *link* the Hopf orbit [16]. Hence any unstable orbit which merges with the period doubled orbit must also link the Hopf orbit. This is a global constraint which is not visible in the Poincaré map. An unstable orbit existing a "distant" region of phase

space, away from the initial period doubling event, will not link the Hopf orbit. This prevents such an unstable orbit from drifting onto the period doubled orbit and facilitating a saddle-node bifurcation.

Obtaining the unstable orbit required for a saddle-node bifurcation is thus somewhat involved because no correctly linked orbits exist initially—they must be created in separate bifurcations. One way this could happen is for the Hopf orbit to period double again, producing an unstable period doubled orbit which is correctly linked with the Hopf orbit. Then the stable period doubled orbit and the newly created unstable period doubled orbit could annihilate each other in a saddle-node bifurcation. If we represent the orbits involved by their Floquet multipliers, this sequence of events is diagrammed in fig. 20. It is amusing to note that this process results in an attracting torus, enclosing the Hopf orbit. For the systems we are emphasizing, this mechanism for producing a correctly linked unstable orbit is not feasible because of the strong dissipation assumption in eq. (6). From fig. 20, the Floquet multipliers of the Hopf orbit would have to satisfy

$$\rho_1 \rho_2 > 1$$

at criticality. This requires

$$\int_0^T \text{div} V_\mu(x_{\text{Hopf}}(t)) dt > 0,$$

which violates eq. (6).

If the desired unstable orbit cannot come from the Hopf orbit, it must be *created* in an independent saddle-node bifurcation. Such a bifurcation could *produce* a stable orbit *and* an unstable orbit; both linking the Hopf orbit. The new orbits would be connected by the unstable manifold of the new unstable orbit. Following this preparatory bifurcation, the new unstable orbit could undergo a saddle-node bifurcation with the stable period doubled orbit, eliminating both of them. If this happened, the surviving stable orbit would become the boundary of the unstable manifold of the Hopf orbit. The net result would be to preserve the Möbius structure of the global flow with the stable

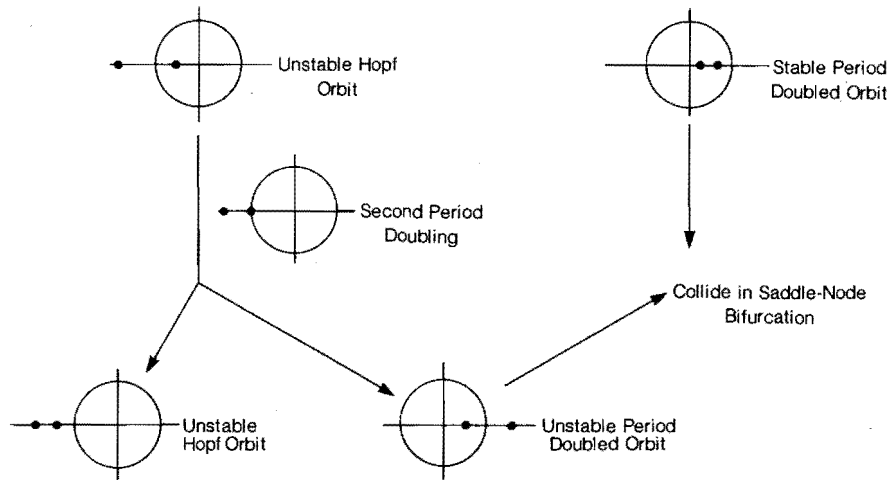


Fig. 20. A bifurcation path after period doubling.

orbit replacing the stable period doubled orbit as the attractor. Experimentally, one might observe this transition as a jump in the frequency and amplitude of the oscillation.

The bifurcation process just described, though certainly feasible, is elaborate, and its complexity is a direct consequence of the global constraints imposed by the period doubled flow. The third and final bifurcation open to the stable period doubled orbit is simple: it could period double as well. This would create a second layer of Möbius flow within the first. Consequently in considering what the *new* period doubled orbit could do, we have only to reiterate the analysis of this section.

In summary, the stable period doubled orbit could undergo a saddle-node bifurcation or it could period double. The saddle-node bifurcation is hindered (though not prohibited) by the global structure of the flow near the period doubled orbit. In this sense the second period doubling bifurcation is easier, and we have the result that a period doubled orbit is “pre-disposed” to period double again.

6. Implications for topology of orbits

Next we would like to understand how the resulting stable multiply-period-doubled orbit is

embedded in \mathbb{R}^3 . In particular are more exotic embeddings than those described in the previous section possible? For this discussion we will need some concepts from elementary knot theory [5, 13]. For Euclidean spaces of more than 3 dimensions, all one dimensional knots are trivial.

A *torus knot*, denoted $T_{p,q}$, is a closed curve embedded in \mathbb{R}^3 on the surface of a torus, winding p times around toroidally and q times around meridionally,

$$\begin{aligned} T_{p,q} &= \{(r, \theta, z) \\ &= (1 + \tfrac{1}{2} \cos 2\pi qt, 2\pi pt, \tfrac{1}{2} \sin 2\pi qt) | t \in [0, 1] \\ &\text{and } (r, \theta, z) \in \mathbb{R}^3\}. \end{aligned}$$

A simple case is $T_{2,1}$ which in fact is not knotted and may be unwrapped into a simple circle. Fig. 21 shows the everyday trefoil to be $T_{2,3}$ and the beautiful “Solomon’s Seal” to be $T_{2,5}$. If p and q are relatively prime integers then one may construct a $T_{p,q}$. A theorem of O. Schreier shows that all torus knots with $1 < p < q$ are topologically distinct [5].

An *iterated torus knot* is obtained by: 1) thickening the “string” of a torus knot to a “rope” (solid torus) fig. 22; 2) considering a torus knot drawn on the toroidal surface of this rope; and 3) iterating this procedure a finite number of times.

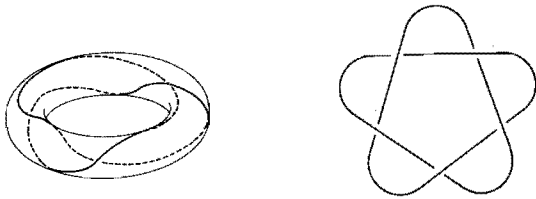


Fig. 21. The trefoil knot (at left) and Solomon's seal knot (at right) as torus knots.

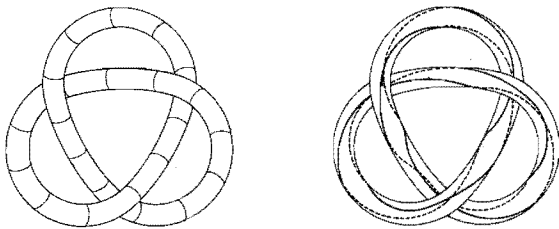


Fig. 22. The trefoil is expanded into a "rope" and an iterated torus knot is drawn on its surface.

In this language the stable period doubled orbit L constructed in the previous sections is topologically equivalent to the torus knot $T_{2,1}$; see fig. 3b. Repeating the construction, to get successive period doublings as indicated at the end of section 4, will produce a stable orbit which is an iterated torus knot of type $T_{2,1}$ at each stage of iteration. By changing the sense of ϕ in fig. 4 one easily sees how to construct $T_{2,-1}$ at any stage. We now demonstrate that in fact there is a sequence of bifurcations which produce a stable orbit that is any iterated torus knot which is of type $T_{2,n}$ with n any odd integer at each stage.

The trick is to alter the flow (for μ between μ_4 and μ_5) so that the eigenvalues rotate around the origin $n/2$ times as in fig. 23. It is easy to see geometrically what is happening to the flow as we do this. Imagine taking the toroidal bag T , slicing it at $\theta = 0$ and twisting the two pieces relative to one another by an angle of $2n\pi$, see fig. 24. The flow keeps track of how much rotation we have performed because the integral curves twist around the central axis of the toroidal bag. The induced map on a Poincaré section, however, does not notice the difference between rotation by 2π and

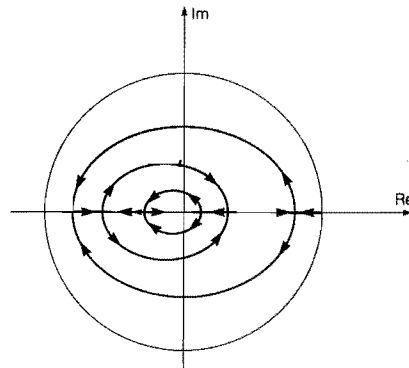


Fig. 23. The path of eigenvalues for a knotted orbit with three half-twists. It can happen that all three circular paths coincide at one radius [11].

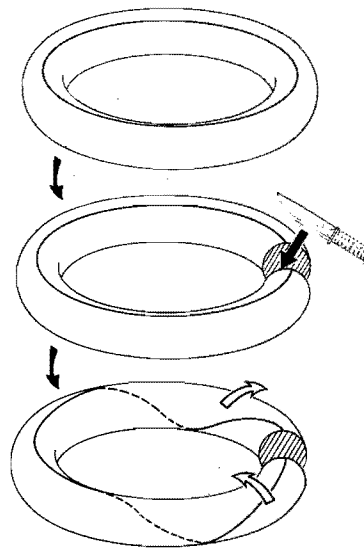


Fig. 24. The effect of twists on the toroidal bag T .

no rotation at all. The one-parameter family of maps induced from such a family of highly twisted flows would be unstable to perturbation were it not for the fact that they arise as Poincaré sections. The family of maps could be perturbed to fig. 25 since eigenvalues are indistinguishable; however such a perturbation is clearly prohibited topologically in the family of flows. Thus a structurally unstable one-parameter family of maps may be stabilized by regarding it as Poincaré sections

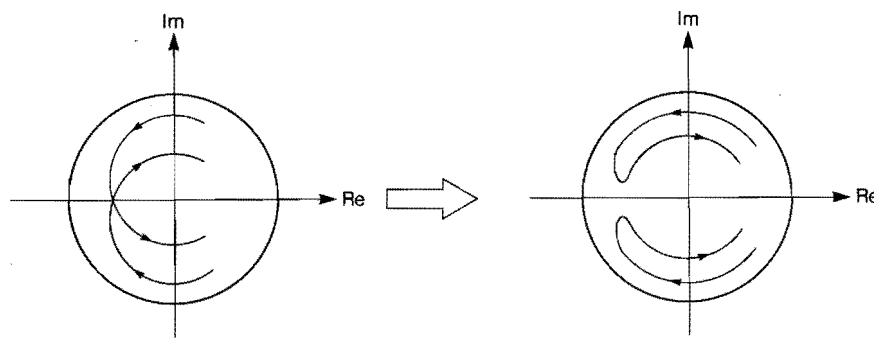


Fig. 25. The effect on the eigenvalue paths of a small perturbation to the family of Poincaré maps. This kind of perturbation to the map cannot arise from a perturbation of the underlying flow.

of a one-parameter family of flows. This is a general phenomenon to be aware of, and indicates a danger in forgetting the flow origins of Poincaré maps.

One may also apply this multiple twist construction at the k th stage of period-doubling. As described at the end of section 4 we choose a toroidal bag surrounding the $k-1$ st period doubled orbit within which the flow is topologically the same as that at the first stage. We allow our one-parameter family to alter the flow only within this bag and follow the prescription of the first stage.

This procedure clearly works for a *finite* number of stages of period doubling. Given an infinite sequence which forms the well-known cascade, it is not clear whether one obtains a smooth 1-parameter family of vector fields. Which knot sequences appear in smooth families is an open question. Numerical studies by two groups have examined this problem for a parametrically driven oscillator [11], a forced Duffing oscillator [11], the forced Brusselator equations [17], and the Lorenz equations [17]. For the parametric and Duffing oscillators, the knot sequences begin as $T_{2,1}$, $T_{2,1}$, $T_{2,3}$, $T_{2,5}$, $T_{2,11}$, $T_{2,21}$, $T_{2,43}, \dots$, and $T_{2,5}$, $T_{2,9}$, $T_{2,19}$, $T_{2,37}$, $T_{2,75}$, $T_{2,149}, \dots$ respectively. For the Brusselator and the Lorenz equations, the initial sequence is $T_{2,1}$, $T_{2,3}$, $T_{2,5}$, $T_{2,11}$, $T_{2,21}$, $T_{2,43}$, $T_{2,85}, \dots$ and $T_{2,1}$, $T_{2,1}$, $T_{2,3}$, $T_{2,5}$, $T_{2,11}, \dots$ respectively. If these sequences in fact reflect asymptotic behavior,

then they all follow a pattern of the form [11]

$$T_{2, N_n(m)} \quad \text{where } n = 1, 2, 3, \dots$$

and

$$N_n(m) = [(3m+2)2^{n-1} + (-1)^{n-1}]/3.$$

The above examples are characterized by either $m=2$ (Lorenz, Brusselator, parametric oscillator) or $m=4$ (Duffing oscillator).

If two sequences of period doublings differ at *any* stage in the knots produced (and their linkings with previous knots) they are topologically different flows. This demonstrates the existence of a countable infinity of topologically distinct period doubling flows. If *all* sequences of knots arise in smooth families of vector fields then in fact there is an uncountable infinity of such period doubling flows. Under this assumption we may develop the following intriguing picture. If, in analogy to the theory of period doubling maps, one could define a renormalization group type operator R in the space of flows then conceivably these knotted period doubling sequences are represented by

1) an infinite number of fixed points of R (where the knot is $T_{2,n}$ at each stage for different n 's);

2) an infinite number of periodic orbits of R of each period (eg. period 2 is $T_{2,n}$; $T_{2,m}$; $T_{2,n}$; $T_{2,m}$; \dots $m \neq n$);

3) chaotic renormalization orbits (T_{2,n_k} , where n_k is a random sequence).

Notice that all these different flows have the *same* Poincaré section.

7. Power spectrum for the knotted orbit

In the experimental analysis of systems exhibiting a transition to turbulent behavior, the structure of the power spectrum, computed by Fourier analyzing a time series, is a useful diagnostic. When a system, oscillating with period T_0 and frequency $\omega_0 = 2\pi/T_0$, period doubles to an oscillation with period $2T_0$, it is expected that the power spectrum will show a new peak at $\omega = \omega_0/2$. Here we consider how the spectrum of the knotted orbit $T_{2,n}$, occurring in our example, depends on the index n . This is interesting because it provides an exception to the intuition "period doubling requires frequency halving", albeit in the context of a carefully constructed example.

For arbitrary $n = 1, 3, 5, \dots$, eqs. (4) become

$$\begin{aligned}\dot{\sigma} &= \eta\sigma + \sigma \left[(\alpha - \eta) \sin^2 \left(\phi - \frac{n\theta}{2} \right) \right. \\ &\quad \left. - \sigma^2 \cos^4 \left(\phi - \frac{n\theta}{2} \right) \right], \\ \dot{\phi} &= \frac{n}{2} + \frac{1}{2} \left[\alpha - \eta + \sigma^2 \cos^2 \left(\phi - \frac{n\theta}{2} \right) \right] \\ &\quad \times \sin 2 \left(\phi - \frac{n\theta}{2} \right), \\ \dot{\theta} &= 1.\end{aligned}$$

Here, along the period doubled orbit, the twists in ϕ are equally spaced in θ ,

$$\phi = \frac{n}{2}\theta,$$

so the angular motion is easily solved:

$$\theta = t, \quad \phi = (n/2)t.$$

Now the (x, y, z) coordinates of the orbit are

$$\begin{aligned}x(t) &= [r_H + \sigma_0 \cos \phi(t)] \cos \theta(t), \\ y(t) &= [r_H + \sigma_0 \cos \phi(t)] \sin \theta(t), \\ z(t) &= \sigma_0 \sin \phi(t),\end{aligned}$$

where r_H is amplitude of the Hopf orbit and σ_0

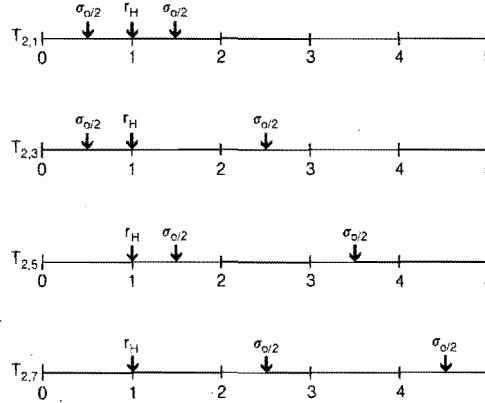


Fig. 26. Possible power spectra for the flows with period doubled orbits $T_{2,1}$, $T_{2,3}$, $T_{2,5}$, and $T_{2,7}$.

the amplitude of the period doubled orbit relative to the Hopf orbit.

All the basic frequencies of the $T_{2,n}$ orbit are exhibited by $x(t)$ which can be rewritten,

$$x(t) = r_H \cos t + \frac{\sigma_0}{2} \left[\cos \left(1 - \frac{n}{2} \right) t - \cos \left(1 + \frac{n}{2} \right) t \right].$$

There are three Fourier components; one at the original frequency $\omega_0 = 1$ with amplitude r_H , and two "sidebands" at $\omega = |1 \pm n/2|$ with amplitude $\sigma_0/2$. The resulting power spectra are shown in fig. 26 for $T_{2,1}$, $T_{2,3}$, $T_{2,5}$, and $T_{2,7}$.

One interesting feature of fig. 26 is that, although the basic period of all these knotted orbits is 4π , the corresponding frequency of $\frac{1}{2}$ does not appear in the spectrum for $n \geq 5$. Of course in applications the vector fields are not written in such simple coordinates and the relationship to our coordinates is likely to be highly nonlinear. This nonlinearity will inevitably cause a Fourier component at $\omega = \frac{1}{2}$ to appear as a beat frequency of the fundamental dynamical frequencies.

8. Possible mechanism for non-universal structure in the asymptotic power spectrum

An important feature of period doubling cascades in maps is the existence of universal

scaling laws in both phase space and parameter space. In parameter space, the point of the n th doubling, μ_n , asymptotically approaches the accumulation value μ_∞ as

$$\mu_\infty - \mu_n \underset{n \rightarrow \infty}{\approx} \delta^{-n}, \quad \text{where } \delta \approx 4.67. \quad (7)$$

In phase space, the distance d_n between adjacent points of the 2^n -cycle rescales in a self-similar fashion as

$$\frac{d_n}{d_{n+1}} \underset{n \rightarrow \infty}{\approx} -\alpha, \quad \text{where } \alpha \approx 2.5. \quad (8)$$

When passing from a period doubling Poincaré map to the flow which defines the map, the geometric convergence of the cascade in eq. (7) will not be altered. It is natural to seek an extension of eq. (8) to the flow as well. Feigenbaum has suggested perhaps the simplest possibility [12]. Let $X_n(t)$ denote the stable period doubled orbit after the n th doubling; it has period $T_n \approx 2T_{n-1}$. In an appropriately chosen Poincaré section, $X_n(t)$ is represented by a 2^n cycle which is generated as the orbit returns to the section in intervals of approximate duration $T_0 \approx T_n/2^n$. The displacement of two adjacent elements of the 2^n -cycle, analogous to d_n , is

$$\psi_n(t) \equiv X_n(t) - X_n(t + T_n/2). \quad (9)$$

Feigenbaum proposes that eq. (8) for the map is replaced by

$$\psi_{n+1} \underset{n \rightarrow \infty}{\approx} \sigma(t/T_{n+1})\psi_n(t), \quad (8')$$

where $\sigma(x)$ is a universal function which is independent of n and satisfies

$$\sigma(x) = -\sigma(x + \frac{1}{2}) = \sigma(x + 1).$$

The time evolution of $\psi_n(t)$ is easily pictured in terms of our geometric model. From its definition (9), ψ_n is a vector lying essentially parallel to the unstable manifold of the orbit X_{n-1} which has just period doubled and is now unstable (the Hopf

orbit in our example); $\psi_n(t)$ is oriented approximately perpendicular to $X_{n-1}(t)$. If the n th doubling produced a T_{2,q_n} torus knot then, *relative* to the unstable orbit X_{n-1} , ψ_n rotates q_n times during an interval $\Delta t = T_n$. Similarly if the $(n+1)$ st doubling produces a $T_{2,q_{n+1}}$, then *relative* to $X_n(t)$, ψ_{n+1} rotates q_{n+1} times during $\Delta t = T_{n+1} \approx 2T_n$. Eq. (8') requires that $\sigma(t/T_{n+1})$ modulate the $2q_n$ oscillations of ψ_n (in $\Delta t = T_{n+1}$) to coincide with the q_{n+1} oscillations of ψ_{n+1} . Moreover $\sigma(x)$ must effect this rescaling between ψ_{n+1} and ψ_{n+2} and so on. This clearly requires some fixed relationship between the pairs of knots $(T_{2,q_n}, T_{2,q_{n+1}})$, $(T_{2,q_{n+1}}, T_{2,q_{n+2}})$, $(T_{2,q_{n+2}}, T_{2,q_{n+3}})$, etc.

These observations allow two conclusions regarding the validity of eq. (8'). First, if eq. (8') applies to a *particular* period doubling cascade, then for that cascade the sequence of knots $\dots T_{2,q_n}, T_{2,q_{n+1}}, T_{2,q_{n+2}}, \dots$ should, as $n \rightarrow \infty$, settle down into some simple "binary" pattern. Second, if $\sigma(x)$ is indeed *universal* over period doubling flows then this asymptotic knot pattern must be universal.

Feigenbaum has shown the scaling behavior of (8') implies a self-similar structure for the power spectrum of the flow at $\mu = \mu_\infty$. If σ is a universal function, then this limiting spectrum will also be universally observed. Thus the question of whether the asymptotic knot sequence is simple and universal is of direct experimental interest.

Acknowledgements

We would like to thank John Rice for suggesting iterated torus knots in this context and Phil Holmes and Bob Williams for interest, comments, and encouragement.

References

- [1] A selection of experiments reporting period doubling. In Rayleigh-Bénard convection: A. Libchaber and J. Maurer, J. de Phys. Lett. 40 (1979) L419; J. Gollub, S. Benson and J. Steinman, Ann. N.Y. Acad. Sci. 357 (1981) 22; M.

- Giglio, S. Musazzi and U. Perini, Phys. Rev. Lett. 47 (1981) 243. In surface waves: R. Keslin, L.A. Turkevich, S.J. Putterman, I. Rudnick, and J.A. Rudnick, Phys. Rev. Lett. 47 (1981) 1133; R.P. Lindsay, Phys. Rev. Lett. 47 (1981) 19. In chemical reactions: R.H. Simoyi, A. Wolf and H.L. Swinney, Phys. Rev. Lett. 49 (1982) 245. In electrical circuits: J. Testa, J. Perez and C. Jeffries, Phys. Rev. Lett. 48 (1982) 714.
- [2] O.E. Rössler, Phys. Lett. 57A (1976) 196. J. Crutchfield, D. Farmer, N. Packard, R. Shaw, G. Jones and R.J. Donnelly, Phys. Lett. 76A (1980) 1. J.M. Wersinger, J. Finn and E. Ott, Phys. Fluids 23 (1980) 1142.
- [3] P. Collet and J.P. Eckmann, Iterated Maps on the Interval as Dynamical Systems (Birkhäuser, Boston, 1980).
- [4] J. Guckenheimer and P. Holmes, Nonlinear Oscillations, Dynamical Systems, and Bifurcations of Vector Fields (Springer, New York, 1983).
- [5] C. Kosniowski, A First Course in Algebraic Topology (Cambridge Univ. Press, Cambridge, 1980). D. Rolfsen, Knots and Links (Publish or Perish, Berkeley, 1976).
- [6] J.E. Marsden and M. McCracken, The Hopf Bifurcation and Its Applications (Springer, New York, 1976). B.D. Hassard, N.D. Kazarinoff and Y-H. Wan, Theory and Applications of Hopf Bifurcation (Cambridge Univ. Press, Cambridge, 1981).
- [7] J. Palis and W. de Melo, Geometric Theory of Dynamical Systems: An Introduction (Springer, New York, 1982).
- [8] This is a well-known result; see for example ref. 4 or J. Mallet-Paret and J. Yorke, Proc. New York Acad. Sci. Meeting on Nonlinear Dynamics (1979).
- [9] J.B. McLaughlin, J. Stat. Phys. 24 (1981) 375. M. Feigenbaum, Los Alamos Science, Summer Issue (1980) 4.
- [10] D. Jordan and P. Smith, Nonlinear Ordinary Differential Equations (Oxford Univ. Press, Oxford, 1977).
- [11] P. Beiersdorfer, J.M. Wersinger and Y. Treve, Phys. Lett. 96A (1983) 269.
- [12] M. Feigenbaum, Commun. Math. Phys. 77 (1980) 65.
- [13] For another application of knots to dynamical systems, see J.S. Birman and R.F. Williams, Knotted Periodic Orbits in Dynamical Systems - I: Lorenz's Equations, Topology 22 (1983) 47-82.
- [14] After this work was completed we learned of the related work: P. Holmes and D. Whitley (1983) Bifurcations of one and two dimensional maps, preprint. D. Whitley (1983) On the Limit of Successive Period-doublings in Diffeomorphisms of the Plane, preprint.
- [15] J.C. Alexander and James A. Yorke, J. Diff. Eqs. 49 (1983) 171.
- [16] K. Alligood, J. Mallet-Paret and J. Yorke, J. Diff. Geom. 16 (1981) 483.
- [17] T. Uezu, Phys. Lett. 93A (1983) 161; T. Uezu and Y. Aizawa, Prog. Theo. Phys. 68 (1982) 1907. These authors note that period doubled orbits may form torus knots, but do not consider iterated torus knots. They define a "relative torsion number" which corresponds to our knot index n in $T_{2,n}$.